LARGE DISPLACEMENT *J*-INTEGRAL DOUBLE CANTILEVER BEAM (DCB) TEST METHOD FOR MODE I FRACTURE TOUGHNESS

by

Joshua Gunderson

A thesis

submitted in partial fulfillment

of the requirements for the degree of

Master of Science in Mechanical Engineering

Boise State University

December 2020

BOISE STATE UNIVERSITY GRADUATE COLLEGE

DEFENSE COMMITTEE AND FINAL READING APPROVALS

of the thesis submitted by

Joshua Gunderson

Thesis Title: Large Displacement *J*-Integral Double Cantilever Beam (DCB) Test Method for Mode I Fracture Toughness

Date of Final Oral Examination: 30 July 2020

The following individuals read and discussed the thesis submitted by student Joshua Gunderson, and they evaluated their presentation and response to questions during the final oral examination. They found that the student passed the final oral examination.

Peter Müllner, Ph.D.	Chair, Supervisory Committee
Anthony Paris, Ph.D.	Co-chair, Supervisory Committee
Mahmood Mamivand, Ph.D.	Member, Supervisory Committee
Joe Guarino, Ph.D.	Member, Supervisory Committee

The final reading approval of the thesis was granted by Peter Müllner, Ph.D., Chair of the Supervisory Committee. The thesis was approved by the Graduate College.

DEDICATION

This work is dedicated to my wife, Crystal. Thank you for sacrificing with me.

ACKNOWLEDGEMENTS

This thesis would not been completed without the support of many friends and colleagues. I am indebted chiefly to Dr. Anthony Paris for his enduring patience, support, and friendship. Without his guidance and encouragement this work would not have been possible.

I am grateful to Phil Boysen for the machining of custom fixtures used in the experimental tests, Dr. Peter Müllner for editing, James Stevenson for assistance with data acquisition and software configuration, and Mike Kesslor for providing DCB specimens. Valuable contributions were also made by John Brueck with early work on the project and Benjamin Murphy with data processing assistance. I would like to extend my thanks to other members of my thesis advisory team for their support of this work.

Finally, I cannot forget the encouragement bordering on harassment received from friends and family to stay the course and see this project through. I cannot list each of you by name, but I would be remiss not to mention my wife Crystal, my mother-in-law Rose, my father Jess, my dear friend Rick Schell, and my long-time mentor Bill Harvey.

ABSTRACT

The *J*-integral is used to develop an alternative double cantilever beam (DCB) test method for the Mode I fracture toughness suitable for both small and large displacements. The current focus is the experimental determination of the Mode I interlaminar fracture toughness of composite materials, but the method is generally applicable to other similar tests and material systems, such as to the Mode I fracture toughness of adhesives. A series of five identical specimens are tested to compare the linear-elastic fracture mechanics method recommended by ASTM, which makes use of linear beam theory with root rotation, large displacement, and end block corrections, with the new nonlinear-elastic and elastic-plastic fracture mechanics method, which does not require these corrections. Experimental results show excellent agreement between the two methods over a series of five tests of primarily linear-elastic DCB specimens subjected to moderate to large displacements as defined in the ASTM standard. Furthermore, an agreement is found between the results of the derivations for the two methods being compared, whereby the large displacement equation for J_{Ic} presented in this work is identical to the equation given by J. G. Williams (1987) and which he found to be the true value of G_{Ic}. It is the true value of G_{Ic} that the large displacement and root rotation correction factors were intended to approximate, and the test method presented here allows for direct measurement of its parameters and evaluation. This method has the added benefit that specimens can be primarily linear-elastic or nonlinear-elastic at the crack tip and may extend to those that are elastic-plastic at the crack tip.

TABLE OF CONTENTS

LIST OF TABLES

LIST OF FIGURES

LIST OF ABBREVIATIONS

ASTM	American Standard for Testing and Materials
cor	correction
DCB	double cantilever beam
eq.	equation
eqs.	equations
LEFM	linear-elastic fracture mechanics
MBT	modified beam theory
std. dev.	standard deviation

CHAPTER 1: INTRODUCTION AND MOTIVATION

The most widely used method of determining Mode I interlaminar fracture toughness in a composite material is the double cantilever beam (DCB) test (ASTM D5528-13). The ASTM recommended modified beam theory (MBT) method is based in linear-elastic fracture mechanics (LEFM) theory (Griffith, 1920; Irwin, 1948; Irwin and Kies, 1952 and 1954; Orowan, 1950) and calculates G_{Ic} using a visual measurement of the crack length as well as measurements of the applied load, load point displacement, and initial specimen geometry.

Motivation for using the *J*-integral comes from the problematic cost, accuracy, and rate of data acquisition inherent in crack length measurement, as well as the limited application of MBT to primarily linear-elastic specimens. The current ASTM test method requires the applied load and load point displacement to be recorded as well as instantaneous location of the delamination front. Typically, visual measurements of the crack front are acquired using a traveling microscope or other visual means, though visual methods can experience inaccuracies due to crack tunneling. The equipment and automation commonly used to monitor crack front location tends to be expensive and prone to error. Manual recording of crack front locations and manual validation or correction of automated measurements are labor intensive. In addition to the data acquisition challenges during testing, the test is limited to specified constraints on specimen size and the assumption of small displacements. Correction factors for end blocks and large displacements provided in the ASTM standard extend these limitations,

but also add complexity in post processing and introduce additional sources of uncertainty. The *J*-integral has been shown (Paris and Paris, 1988) to reveal alternative formulations for the DCB Mode I interlaminar fracture toughness which do not depend upon knowledge of the crack front location and which are not limited by the full set of constraints associated with MBT.

Prior efforts have produced preliminary data that show for a small displacement analysis of the DCB specimen the *J*-integral produces experimental results similar to the LEFM based ASTM method (Gunderson, Brueck, and Paris, 2007). The present work extends the equations developed for G_{Ic} and J_{Ic} to accommodate large displacements and nonlinear materials and carries out a series of DCB Mode I fracture toughness tests with moderate to large displacements to show whether the results using G_{Ic} and J_{Ic} are statistically interchangeable.

CHAPTER 2: THEORY

2.1 The DCB Specimen

Figure 1 shows the DCB specimen geometry where a_0 is the original crack length, b is the specimen width, h is the thickness of the specimen, L is total length, and P is the applied load. Figure 2 shows test parameters such as load point displacement δ, crack length a, opening angle θ, and the horizontal distance from the crack tip to the load line $\overline{X}_1$. Both the energy release rate G and the J-Integral (defined below) are evaluated for large displacements for the DCB specimen to ensure a proper comparison of the two approaches. In the literature, there is some variation in nomenclature between authors writing on the same or related subject matter. An attempt has been made here to define and use consistent nomenclature throughout this thesis. This necessitated some deviation from nomenclature used in the referenced literature. Wherever practical, the notation used in the ASTM standard was adopted.

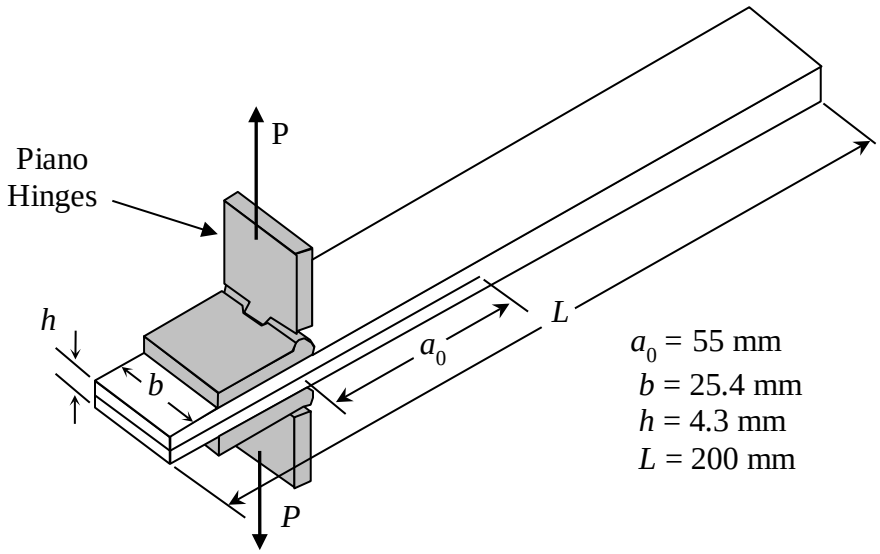

Figure 1 The DCB Specimen.
Specimen geometry is shown where a_0 is the original crack length, b is the specimen width, h is the thickness of the specimen, L is total length, and P is the applied load.

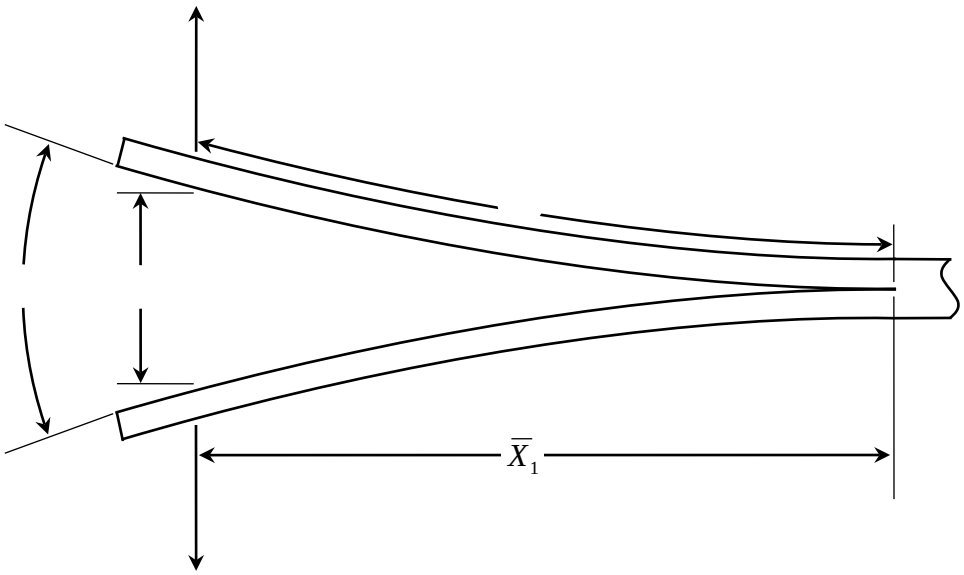

Figure 2 DCB Parameters.
Test parameters are shown including load point displacement δ, crack length a, opening angle θ, and the horizontal distance from the crack tip to the load line $\overline{X}_1$.

2.2 Energy Release Rate *G*

Figure 3 shows a cracked body subject to a single load. The linear-elastic fracture mechanics (LEFM) energy release rate *G* (Irwin 1948; Irwin and Kies, 1952; Irwin and Kies, 1954) can be expressed as

$$G = \frac{P}{b}\frac{\mathrm{d}\delta}{\mathrm{d}a} - \frac{P}{b}\frac{\mathrm{d}U}{\mathrm{d}a} = \frac{1}{b}\frac{\mathrm{d}U}{\mathrm{d}a}\Big|_{P_{const.}} = -\frac{1}{b}\frac{\mathrm{d}U}{\mathrm{d}a}\Big|_{\delta_{const.}}, \quad (1)$$

where a is the crack length, b is the constant body thickness, δ is the load point displacement in the direction of the load, P is the applied load, and U is the strain energy in the body.

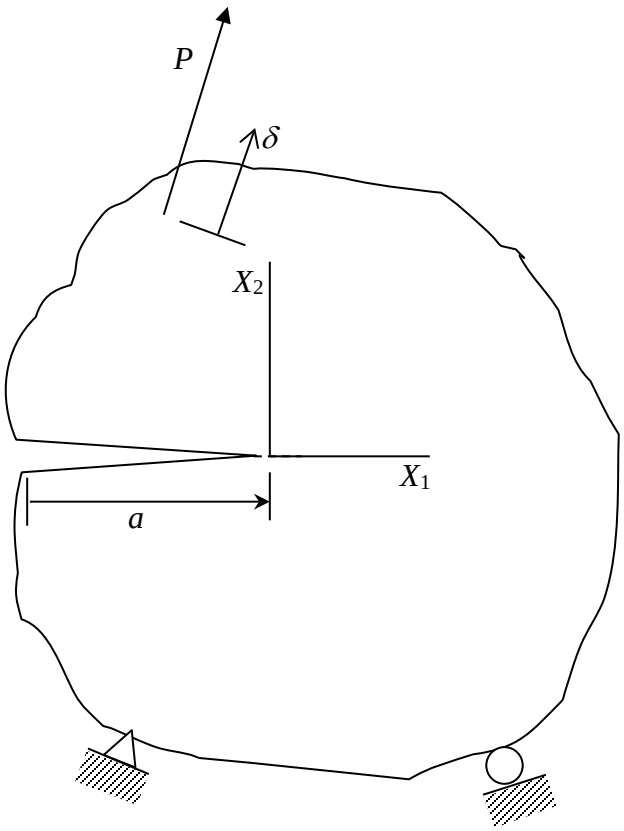

Figure 3 Cracked Body Subjected to Loading.
Shows a cracked body subject to a single load where *a* is the crack length, *b* is the constant body thickness, *P* is the applied load, and *W* is the complementary energy in the body.

The energy release rate *G* may also be expressed in terms of compliance. For a linear-elastic material and geometry, the strain energy *U* is equal to the complementary strain energy *W* in the body, and

$$W = U = \frac{1}{2} P\delta, \tag{2}$$

where δ is the displacement of the loading point in the direction of the load. Equations (1) and (2) and the definition of compliance $C = \delta/P$ yield

$$G = \frac{P^2}{2b}\frac{\mathrm{d}C}{\mathrm{d}a}. \quad (3)$$

This method, known as the *compliance method*, requires an appropriately large number of load, displacement, and crack length measurements such that a third order polynomial approximation may be developed for $C = f(a)$. It does require that the load and displacement are linearly proportional for any given crack length.

The energy release rate G_I may be considered for use as a fracture criterion (Hertzberg, Vinci, and Hertzberg, 2013). Equilibrium is achieved when the crack driving force G_I is equal to the material's resistance R. For a material that is well characterized by an idealized R-curve (that is, the R-curve has a sufficiently sharp corner and is subsequently constant for increasing crack lengths), a critical value of the energy release rate G_{Ic} can be defined. Mode I crack growth begins when $G_I = G_{Ic}$.

Application of Linear-Elastic Fracture Mechanics to the DCB Specimen

The derivation used here relies on a paper by Williams (1987) concerning large displacement and end block corrections. Figure 4 summarizes the primary dimensions necessary for the analysis.

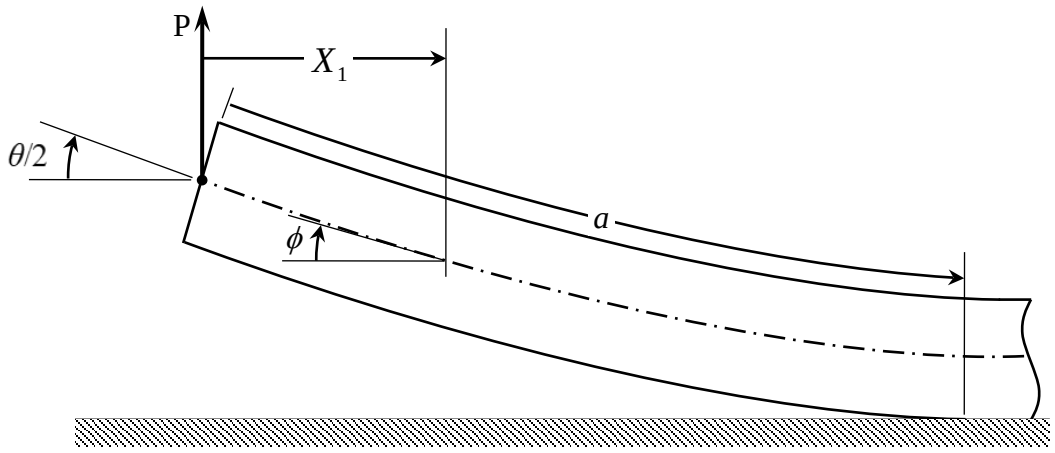

Figure 4 Beam Arm Geometry.
Shown are the primary dimensions necessary for the analysis where P is the applied load, X_1 is the horizontal distance measured from the load line, a is the crack length, θ is the opening angle, and ϕ is the angle of the beam at X_1.

For the loading condition shown, the bending moment M along the beam arm is

$$M = -PX_1, \tag{4}$$

where X_1 is the horizontal distance measured from the load line. Pure bending is assumed such that

$$\frac{1}{R} = \frac{M}{EI}, \tag{5}$$

where R is the radius of curvature of the middle surface, E the axial modulus, and I the second moment of the area for the cross-section.

End or loading block corrections are introduced here in the form of

$$M = -P(X_1 + L' \cos(\theta/2) - t \sin(\theta/2)), \tag{6}$$

where L' and t are defined in Figure 5. When L' and t are small compared with X_1, as may be the case for piano hinges, the corrections may prove to be negligible (ASTM D5528-13).

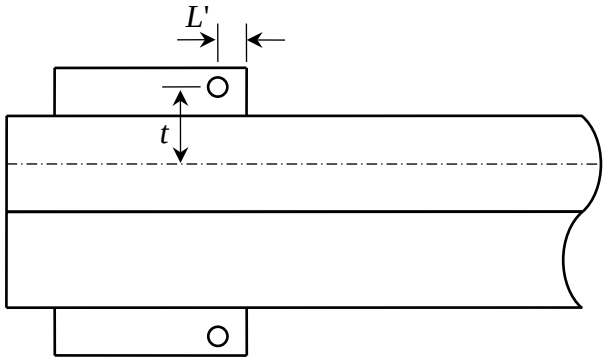

Figure 5 End Block Correction Factor Parameters.
The end block geometry is shown, including parameters *L*' and *t* as defined in ASTM D5528-13.

Combining eqs. (4) and (5) yields

$$R = -\left(\frac{EI}{P}\right)\frac{1}{X_1}. \tag{7}$$

For the differential beam element shown in Figure 6

$$R = \frac{\mathrm{d}\,s}{\mathrm{d}\,\phi} = \frac{\mathrm{d}X_1}{\mathrm{d}\,\phi}\frac{1}{\cos\phi}, \tag{8}$$

where d*s* is the differential distance along the beam's middle surface, ϕ is the angle of the beam element relative to the undeformed orientation at X_1, and dϕ is the differential change in the angle of the beam element. Combining eqs. (7) and (8) and integrating yields

$$\int_0^{\overline{X}_1} X_1 \, \mathrm{d}X_1 = -\left(\frac{EI}{P}\right) \int_{\theta/2}^{0} \cos\phi \, \mathrm{d}\phi. \tag{9}$$

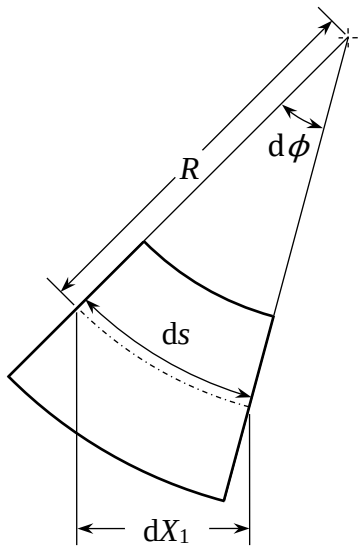

Figure 6 Differential Beam Element Geometry.
Here d*s* is the differential distance along the beam's middle surface, ϕ is the angle of the beam element relative to the undeformed orientation at X_1, and dϕ is the differential change in the angle of the beam element.

where ϕ is the beam angle at the location X_1 and $\overline{X}_1$ is the value of X_1 at the crack tip.

Integrating and solving for $\overline{X}_1$ yields

$$\overline{X}_1 = \left(\frac{2EI \sin(\theta/2)}{P}\right)^{1/2}. \tag{10}$$

where $\theta/2$ is the beam angle at the load point.

If the energy is due to beam bending and the complementary energy is equal to the strain energy, the strain energy *U* and energy release rate can be expressed as

$$W = U = \int_0^a \frac{M^2}{2EI}\,\mathrm{d}s \tag{11}$$

and

$$G_{\mathrm{I}} = \frac{2}{b}\frac{\mathrm{d}}{\mathrm{d}a}\int_0^a \frac{M^2}{2EI}\,\mathrm{d}s = \left.\frac{M^2}{bEI}\right|_{s=a}, \tag{12}$$

where the bending moment at the crack tip due to the applied load is

$$M = -P\bar{X}_1. \tag{13}$$

The result of combining eqs. (10), (12), and (13) is

$$G_{\mathrm{I}} = \frac{2P}{b}\sin(\theta/2)\,. \tag{14}$$

The ASTM standard for this type of test assumes small displacements (linear beam theory), which allows the energy release rate to be calculated by measuring load point displacement and crack length rather than beam angle. The small displacement linear beam theory assumption provides

$$\frac{\delta}{2} = \frac{Pa^3}{3EI} \tag{15}$$

and

$$\overline{X}_1 = a. \tag{16}$$

Combining eqs. (10), (15) and (16) yields

$$\sin(\theta/2) = \frac{3\delta}{4a}. \tag{17}$$

Finally, substituting eq. (17) into eq. (14) yields the familiar

$$G_{\mathrm{I}} = \frac{3P\delta}{2ba}. \tag{18}$$

Here a problem arises due to an incongruity between the actual DCB test specimen and the assumption of a perfectly built-in beam inherent in the linear beam theory. Beam root rotation occurs near the crack tip, for which three methods of correction are provided in the ASTM standard. The modified beam theory (MBT) is recommended in the standard and replaces eq. (18) with

$$G_{\mathrm{I}} = \frac{3P\delta}{2b(a + |\Delta|)}, \tag{19}$$

where the compliance offset Δ is found by plotting the delamination length vs. the cube root of compliance C, where $C = \delta/P$, and finding the value at which a least squares fit line intersects the ordinate. This process is illustrated in Chapter 4.

In addition to root rotation, corrections for large displacement and end block effects must now be considered due to the specimen geometry and material properties used in the present experiment. Corrections for these effects are defined in the ASTM standard and were developed by Williams (1987, 1989) and Hashemi et al. (1989). They modify eq. (19) firstly with an end block correction *N* for load point displacement so that eq. (15) can be rearranged and the compliance becomes

$$\frac{\delta}{P} = \frac{2a^3}{3EI} N. \tag{20}$$

The crack length a must again be adjusted for root rotation, but here the delamination length must be plotted against $C^{1/3} = (\delta/PN)^{1/3}$. The result is a smaller offset, Δ_{cor}. Secondly, eq. (19) also requires a large displacement correction F so that

$$G_{\text{I}} = \frac{3P\delta}{2b(a + |\Delta_{\text{cor}}|)} \frac{F}{N}. \tag{21}$$

The ASTM standard defines large displacements as having $\delta/a > 0.4$.

The two correction factors are given by Williams (1989) as follows:

$$F = 1 - \frac{3}{10}\left(\frac{\delta}{a}\right)^2 - \frac{3}{2}\left(\frac{\delta t}{a^2}\right) \tag{22}$$

and

$$N = 1 - \left(\frac{L'}{a}\right)^3 - \frac{9}{8}\left[1 - \left(\frac{L'}{a}\right)^2\right]\left(\frac{\delta t}{a^2}\right) - \frac{9}{35}\left(\frac{\delta}{a}\right)^2. \tag{23}$$

In the case of a piano hinge, L' may be sufficiently small that N can be approximated by

$$N = 1 - \frac{9}{8}\left(\frac{\delta t}{a^2}\right) - \frac{9}{35}\left(\frac{\delta}{a}\right)^2. \tag{24}$$

Criteria are given in the ASTM standard for the use of the two correction factors. For loading with piano hinges, these criteria together with the specimen geometry call for the use of F, but not N. After observing counter-intuitive differences between the results of experimental data analyses with and without the correction factors as described in the

ASTM standard, a thorough review of the source material (Williams, 1989) revealed deviations of the ASTM standard from the source material. We determined that both *F* and *N* ought to be used to appropriately correct for large displacements, regardless of whether piano hinges or loading blocks were being used, and that the stated purpose in the ASTM standard for each correction factor within the ASTM standard needed clarification. Specifically, the ASTM standard explains that the correction factor *F* accounts for shortening of the moment arm as well as tilting of the end blocks and *N* accounts for stiffening of the specimen. This implies that the correction factor *N* has no terms present to account for large displacement, and thus if beam arm stiffening is not anticipated then the correction factor *N* need not be used. However, Williams derivations of *F* and *N* and an inspection of eqs. (22) and (23) above show that both correction factors contain similar terms which are important to correct for large displacements δ, and thus both *F* and *N* should be used whenever large displacements are present, regardless of whether beam stiffening is likely to occur. We have communicated a proposed change to the ASTM standard and traveled to an ASTM committee meeting to present our proposal (Gunderson and Paris, 2017). The committee has agreed in principle with our findings and plans to consider implementing the proposed change in a future revision to the standard.

The compliance method given by eq. (3) and the polynomial approximation $C = f(a)$ is used as a reference when plotting and comparing G_{Ic} from eq. (21 - 23) and J_{Ic} which is introduced next. Since the compliance method does not rely on linear beam theory, it does not need a root rotation correction (Hashemi et al., 1989).

2.3 *J*-integral

This method makes use of the *J*-integral and the critical value J_{Ic} (Rice, 1968). The *J*-integral as described by Rice considers a two-dimensional strain field applied to a notched body of linear or nonlinear elastic material as shown in Figure 7.

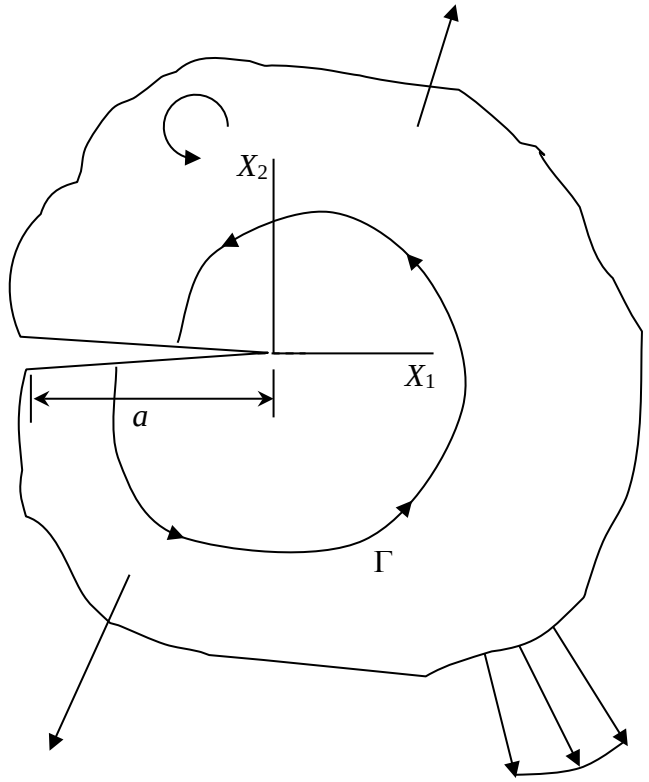

Figure 7 Two-Dimensional Cracked Body Subjected to Loading.
Here Γ is the contour and *a* is the crack length.

The strain energy density *W* is then a function of the stress and strain fields as

$$W = \int_0^{\varepsilon_{ij}} \sigma_{ij} \mathrm{d}\varepsilon_{ij} \tag{25}$$

The *J*-integral is a path independent integral around the crack tip and appears as

$$J_{\mathrm{I}} = \int_{\Gamma} \left(W \mathrm{d}X_2 - \mathbf{T} \cdot \frac{\partial \mathbf{u}}{\partial X_1} \mathrm{d}\Gamma \right), \tag{26}$$

where W is the strain energy density from eq. (25), $\mathbf{T}$ is the traction vector $T_i = \sigma_{ij} n_j$, $\mathbf{n}$ is the outward normal vector to Γ, Γ is the contour, X_1 and X_2 are rectangular coordinates parallel and normal to the crack front respectively, $\mathrm{d}\Gamma$ is the counterclockwise incremental distance along the contour, and $\mathbf{u}$ is the displacement vector. Begley and Landes (1972) demonstrated the use of an experimental method to evaluate J_{I} using the load deflection curves of identical specimens with varying crack lengths. They also explained that both numerical and analytical solutions to the *J*-integral are possible. In this experiment, we employed an analytical solution.

The parameter J_{I} may be used in a Mode I crack growth criterion. Mode I crack growth begins when $J_{\mathrm{I}} = J_{\mathrm{Ic}}$.

Rice (1968) assumed a linear elastic or nonlinear elastic material when proving path independence for the *J*-integral, though he extended the theory to allow for small scale yielding in the vicinity of the crack tip for elastic-plastic materials. The path independent *J*-integral may continue to provide reasonable results when plastic zones extend beyond the vicinity of the crack tip, exceeding the constraints of small scale yielding, so long as the assumptions inherent to the deformation theory of plasticity are valid (i.e. a nonlinear elastic-plastic stress-strain relationship such that the stress tensor is a monotonic function of the strain tensor and loading is proportional to the deviatoric stress components). Additionally, care must be exercised when large scale yielding or large strains are permitted, as adjustments may need to be made to account for specimen

geometry (Anderson, 1991). Increasing plasticity tends to complicate the use of a single parameter to characterize conditions at the crack tip.

Application of the *J*-integral to the DCB Test

Application of the *J*-integral to the Mode I DCB test was first presented by Paris and Paris (1988) who required knowledge of only two measurands, the beam angle and the applied load. However, this derivation relied on the assumption of small displacements throughout the specimen whereas in the present work allowance is made for large displacements. The geometry and material of the DCB specimens considered in this analysis is such that the assumption of small scale yielding is applicable.

The *J*-integral contour and subsequent derivation develop differently depending on where one chooses to account for the applied tractions. Two viable approaches are a horizontal contour segment at the interface between the piano hinge and beam arm shown in Figure 8 (representing a surface in the X_1X_3 plane) and a vertical contour segment at the inward edge of the piano hinge or loading block shown in Figure 9 (representing a surface in the X_2X_3 plane).

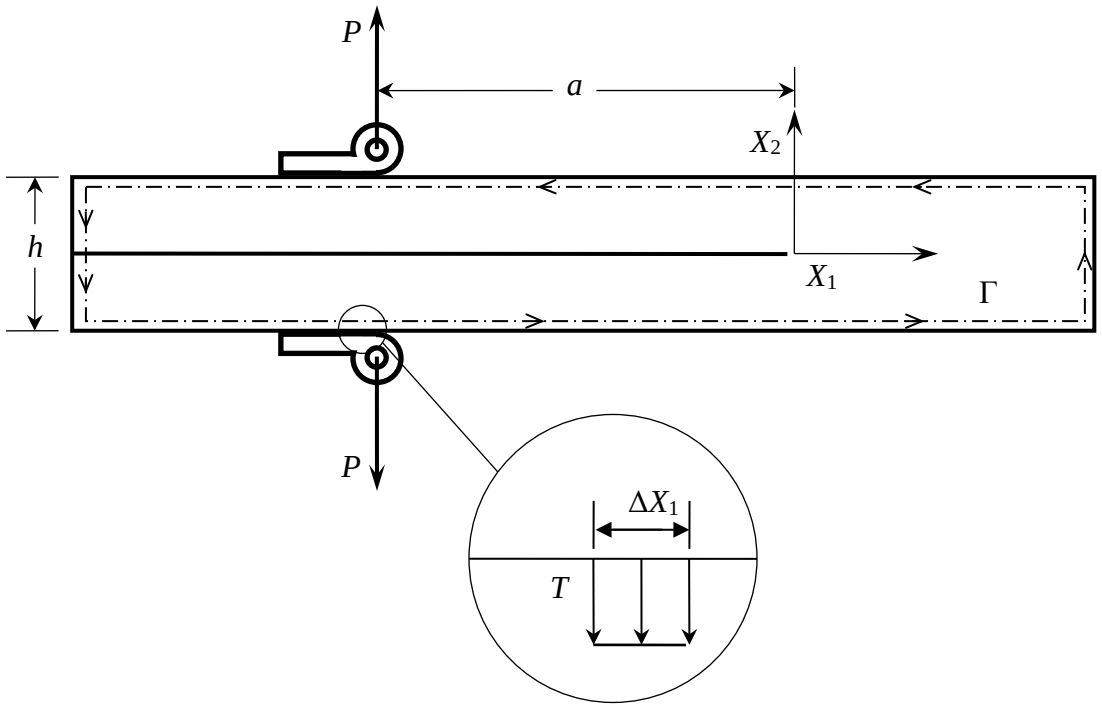

Figure 8 Undeformed DCB Specimen (Tractions on Horizontal Contour Segment).

Here the specimen is depicted in the X_1X_2 plane where P is the applied load, a is the crack length, h is the specimen thickness, T is the applied traction under the piano hinge, Γ is the contour.

J-integral (Horizontal Surface)

Gunderson, Brueck, and Paris (2007) utilized the horizontal surface approach with the assumption that the traction was varying and that the beam curvature throughout the surface was negligible due to hinge stiffness. The following derivation illustrates the horizontal surface approach and instead assumes constant traction and small curvature.

Applying eq. (26) to the DCB specimen shown in Figure 8 yields

$$J_{\mathrm{I}} = 2 \int_{\Delta X_1} T \frac{\mathrm{d}v}{\mathrm{d}X_1} \mathrm{d}X_1. \tag{27}$$

Note that if T is constant eq. (27) becomes

$$J_{\mathrm{I}} = 2T \int_{\Delta X_1} \frac{\mathrm{d}v}{\mathrm{d}X_1}\,\mathrm{d}X_1 = 2T\Delta v b = \frac{2(Tb\Delta X_1)}{b}\frac{\Delta v}{\Delta X_1}, \tag{28}$$

where $\Delta v/\Delta X_1$ is approximately $\sin(\theta/2)$, θ is the total angle between the specimen arms at the load points, and $Tb\Delta X_1 = P$. Equation (28) then becomes

$$J_{\mathrm{I}} = \frac{2P}{b}\sin(\theta/2)\,. \tag{29}$$

If an R-curve is desired, solving eq. (15) for *a*, the *derived crack length*, yields

$$a = \frac{3\delta}{2}\csc(\theta/2)\,. \tag{30}$$

Applying the linear beam theory assumptions to eq. (17) allows the *derived crack length* to be approximated by

$$a = 3\delta/2\theta\,. \tag{31}$$

<u>*J*-Integral (Vertical Surface)</u>

The large displacement derivation presented by Nilsson (2006) uses the vertical surface approach and is applicable for a more generalized loading condition. The following derivation accounts for an application of the load using a piano hinge. Here we generally follow the form of the derivation developed by Nilsson, deviating in the later stages as we apply simplifying assumptions appropriate to the present experiment.

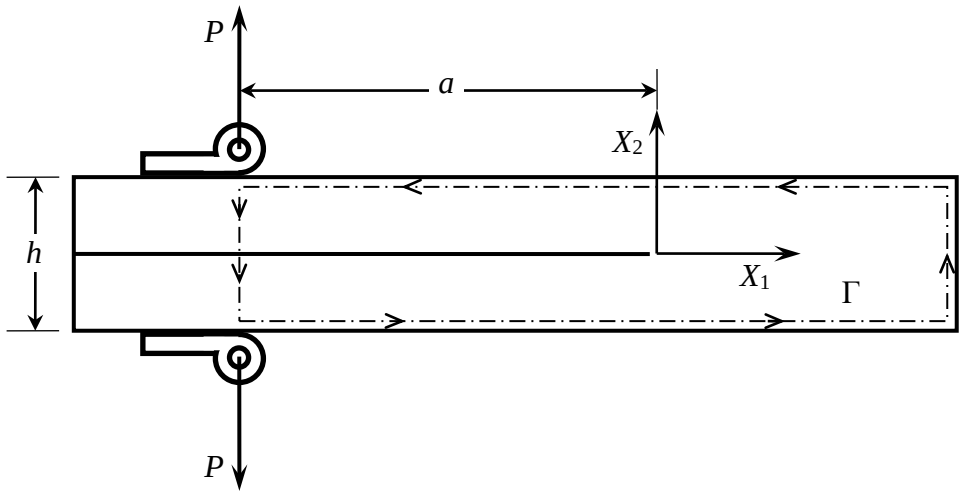

Figure 9 Undeformed DCB Specimen (Tractions on Vertical Contour Segment).

Here the specimen is depicted in the X_1X_2 plane where P is the applied load, a is the crack length, h is the specimen thickness, Γ is the contour.

The J-integral is a path independent line integral around the crack tip and appears as

$$J_{\mathrm{I}} b = \int_S \left(W \delta_{1j} - Q_{ji} \frac{\partial u_i}{\partial X_1} \right) N_j \, \mathrm{d}S \tag{32}$$

using nomenclature similar to that chosen by Nilsson and shown in Figure 9. Here $W = \int \sigma_{ij} d\epsilon_{ij}$ is the strain energy density, δ is the Kronecker Delta, S is the contour surface, X_1 and X_2 are rectangular coordinates parallel and normal to the crack front respectively, dS is the counterclockwise incremental distance along the contour surface, **Q** is the Piola-Kirchhoff stress tensor acting on the contour, **u** is the displacement vector, and **N** is the outward unit normal vector to the contour.

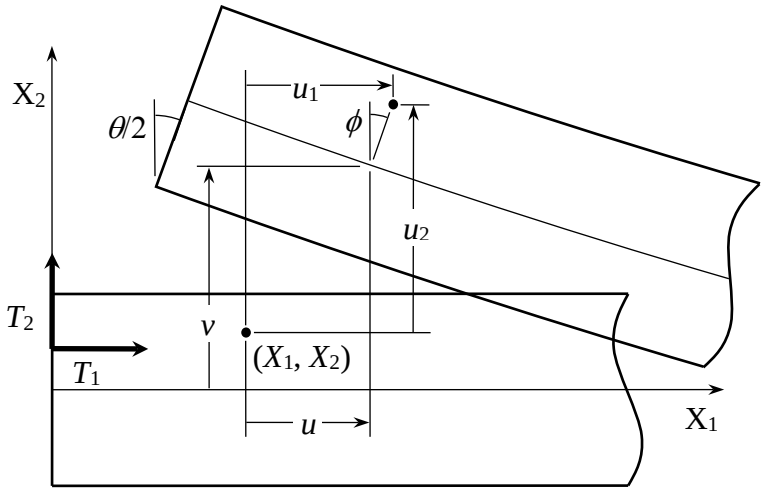

Figure 10 Displacements.

Here u and v are the undeformed displacements of a point on the specimen's neutral axis, u_1 and u_2 are the deformed displacements of an arbitrary point, ϕ is the angle of the beam at an arbitrary point, T_1 and T_2 are the tractions associated with the applied load, θ is the opening angle, and X_1 and X_2 are the undeformed coordinate directions.

The applied load P appears as the set of orthogonal tractions shown in Figure 10 so that

$$Q_{11} = -T_1 \tag{33}$$

and

$$Q_{12} = -T_2. \tag{34}$$

In the undeformed coordinate system

$$\mathrm{d}S = b\mathrm{d}X_2. \tag{35}$$

Observing the geometry of the displacements depicted in Figure 10 yields

$$u_1 = u + X_2 \sin\phi \tag{36}$$

$$u_2 = v - X_2(1 - \cos\phi). \tag{37}$$

The specimen geometry, loading, *J*-integral contour, and eqs. (32-37) yield

$$\frac{J_\mathrm{I} b}{2} = \int_{h/2} \left[W + T_1 \left(\frac{\partial u}{\partial X_1} + X_2 \cos\phi \frac{\partial \phi}{\partial X_1} \right) + T_2 \left(\frac{\partial v}{\partial X_1} - X_2 \sin\phi \frac{\partial \phi}{\partial X_1} \right) \right] b \mathrm{d}X_2. \tag{38}$$

Noting that $\frac{\partial u}{\partial X_1}$, $\frac{\partial v}{\partial X_1}$, and $\frac{\partial \phi}{\partial X_1}$ are constant with respect to X_2 in eq. (38) yields

$$\frac{J_\mathrm{I} b}{2} = \int_{h/2} W\, b \mathrm{d}X_2 + \frac{\partial u}{\partial X_1} \int_{h/2} T_1\, b \mathrm{d}X_2 + \frac{\partial v}{\partial X_1} \int_{h/2} T_2\, b \mathrm{d}X_2 + \frac{\partial \phi}{\partial X_1} \int_{h/2} (T_1 \cos\phi - T_2 \sin\phi) X_2\, b \mathrm{d}X_2. \tag{39}$$

We now deviate from Nilsson's derivation to apply constraints specific to the present experiment. The loading at the vertical surface shown in Figure 9 and Figure 10 can be expressed in terms of the tractions as follows:

$$\int_{h/2} T_1\, b \mathrm{d}X_2 = 0, \tag{40}$$

$$\int_{h/2} T_2\, b \mathrm{d}X_2 = P, \tag{41}$$

and

$$\int_{h/2} (T_1 \cos\phi - T_2 \sin\phi) X_2 \, b \mathrm{d}X_2 = M. \tag{42}$$

Here *M* is the applied moment and *P* is the applied load in the vertical direction. Substituting from eqs. (40-42) into eq. (39) yields the much simpler

$$\frac{J_\mathrm{I} b}{2} = \int_{h/2} W \, b \mathrm{d}X_2 + P \frac{\partial v}{\partial X_1} + M \frac{\partial \phi}{\partial X_1}. \tag{43}$$

If $\theta/2$ is the beam angle at the loading point, then

$$\frac{\partial v}{\partial X_1} = \sin(\theta/2). \tag{44}$$

Finally, if the beam is loaded with piano hinges, $\int_{h/2} W b \mathrm{d}X_2$ and *M* are small, and eq. (43) simplifies to

$$J_\mathrm{I} = \frac{2P}{b} \sin(\theta/2). \tag{45}$$

Regardless of whether the horizontal or vertical contour surface is used to account for the applied load, the *J*-integral analysis results in the same equation for J_I.

CHAPTER 3: MATERIALS AND METHODS

3.1 Test Materials

The specimens were prepared in accordance with the specifications in the standard (ASTM D5528-13) with the exception of slight modifications necessary to facilitate attachment of the angle measurement assemblies and the use of woven fibers rather than unidirectional. The composite material was LTM24ST on woven 7725 glass manufactured using an autoclave process with a curing temperature of 79.4 °C. Referring to Figure 1, the specimen nominal dimensions were a_0 = 55 mm, b = 25.4 mm, h = 4.3 mm and L = 200 mm.

The tensile test machine was a United SFM-30 using an Interface Force Transducer (D11267 SM-100N) with 10V excitation voltage. Angle measurements were obtained using transducers connected to a National Instruments USB-6009 data acquisition unit utilizing LabView 8.0. The transducers were US Digital MA3 absolute magnetic rotary encoders. These would replace the equipment used to measure load point displacement and crack length if the *J*-integral method was used in place of the method prescribed in the current ASTM standard. A photograph of the apparatus is shown in Fig. 11.

3.2 Experimental Procedure

The specific aim of the experiment was to compare the results of five tests to show that G_{Ic} and J_{Ic} are statistically interchangeable. This required that the test methods be carried out simultaneously on each specimen and the data analyzed to determine the degree of agreement between them.

DCB specimens were tested in tension at a rate of 5 mm per minute and a digital video camcorder was used to visually record the delamination length while transducers measured the beam angle, applied load, and load point displacement. The fiberglass/epoxy specimens were translucent, making it possible to make a visual measurement of the crack length from above rather than from the edge. This avoided problems associated with edge measurement as well as crack tunneling. Figure 2 shows the loading geometry of the DCB specimen as well as those parameters not included in Figure 1. Visual, audio, and force markers were used to synchronize the time scale of the digital video with that of the data acquisition unit. Synchronizing was facilitated by matching crack propagation observed on a plot of load vs. time (abrupt drops in applied load) and crack propagation observed in the recorded video. Synchronization offset values were checked by using the load plot to predict the location of sudden crack propagation events as well as the moment when the tensile testing machine's chain drive was activated. If these predicted times corresponded to the appropriate event in the recorded video to within one frame then the offset value was considered to be accurate.

While all the parameters in the equations are important when calculating the fracture toughness, the load and specimen width (provided the width is within tolerances) lose relative importance when attempting to show equivalence between G_{Ic} and J_{Ic} and it

is the crack length, angle, and load point displacement that have the greatest effect on the results. For this reason, extra care was taken to ensure a valid zero condition was used to generate an offset for the raw data in the case of the angle and load point displacement. Zeros for the rotary encoders and load point displacement were facilitated through the use of spring clamps. The clamps were applied to the specimen before and after the piano hinges tending to close the crack after which a load of approximately twenty newtons was gradually applied. This allowed the transducers to record the angle when the specimen was perpendicular to the direction of loading as well as the load as the slack was removed from the hinges. These two values became the zero values for both the angle and the load point displacement.

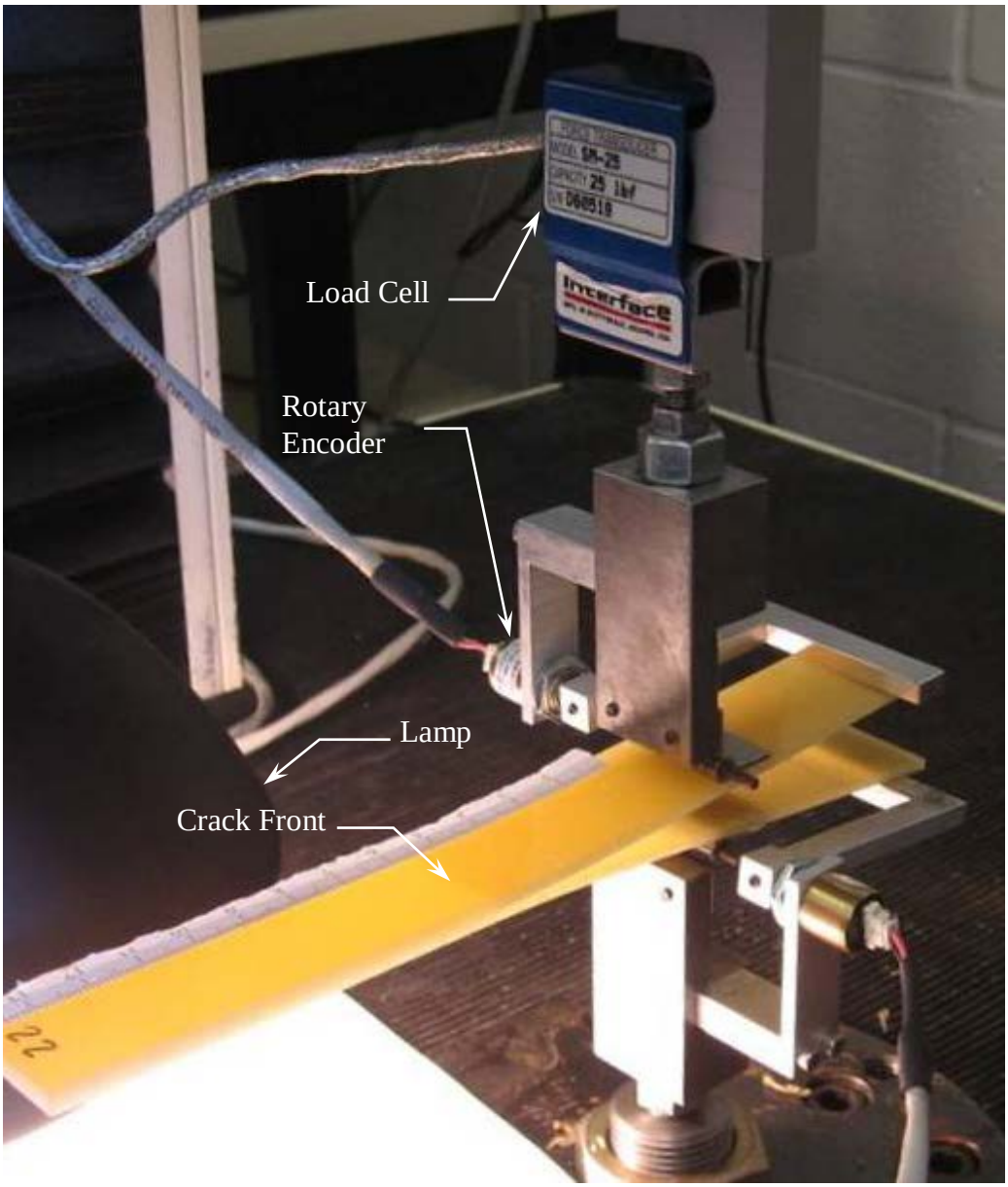

Figure 11 Test Apparatus.
The tensile test machine is shown with a specimen in the DCB fixture. The load cell and rotary encoders are visible. A lamp adjacent to the specimen allows the crack front to be clearly seen in timestamped video recordings.

CHAPTER 4: RESULTS AND DISCUSSION

The data for test 5 is used to illustrate the results. Figure 12 shows load vs. load point displacement, and Figure 13 shows crack length and beam angle vs. load point displacement. In order to show the vertical portion of the R-curve, non-critical ramp-up data points must be included. These ramp-up points are shown in Figure 12 with a unique symbol and they are combined with the critical points in Figure 13 and Figure 15.

Figure 13 compares the measured crack length with the derived crack length calculated using eq. (31). Note that accuracy of the derived crack length improves and becomes sufficient as applied load approaches the critical value. Figure 14 shows crack length vs. cube root of compliance and the method used to determine the compliance offset Δ_{cor} as discussed earlier.

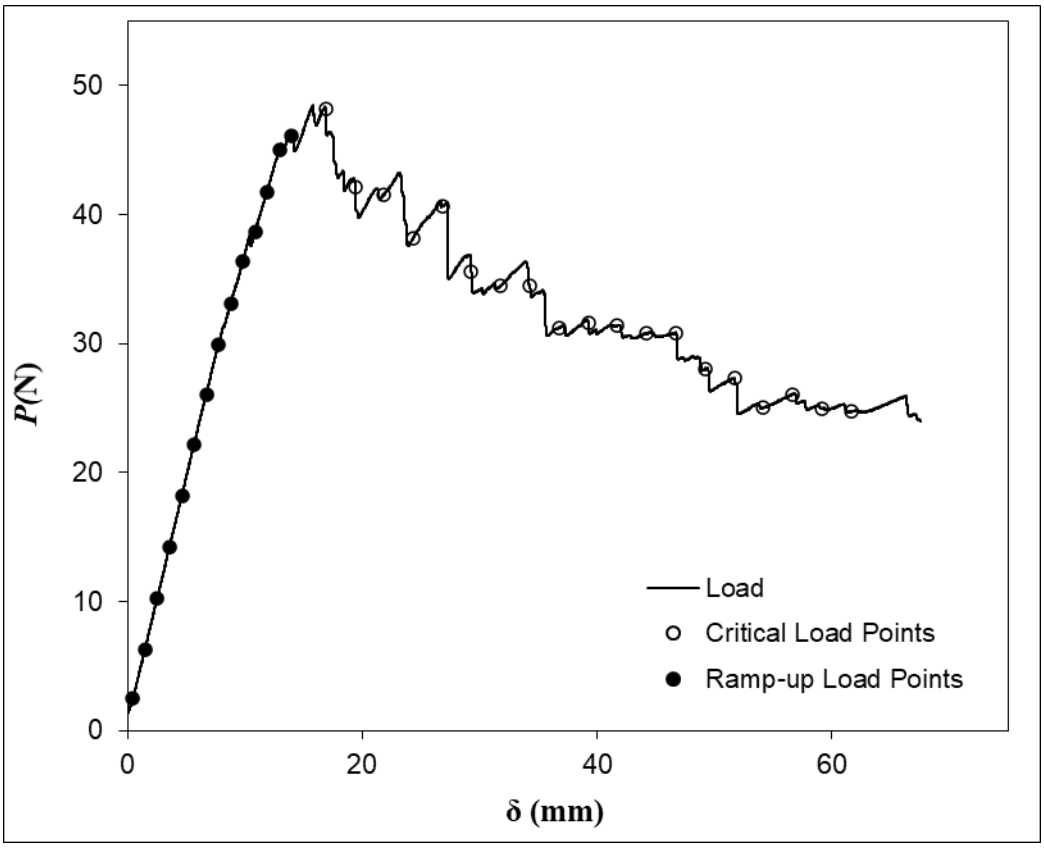

Figure 12 Applied Load vs. Load Point Displacement.
Here P is the applied load and δ is the load point displacement. Both critical load and ramp-up load points are shown.

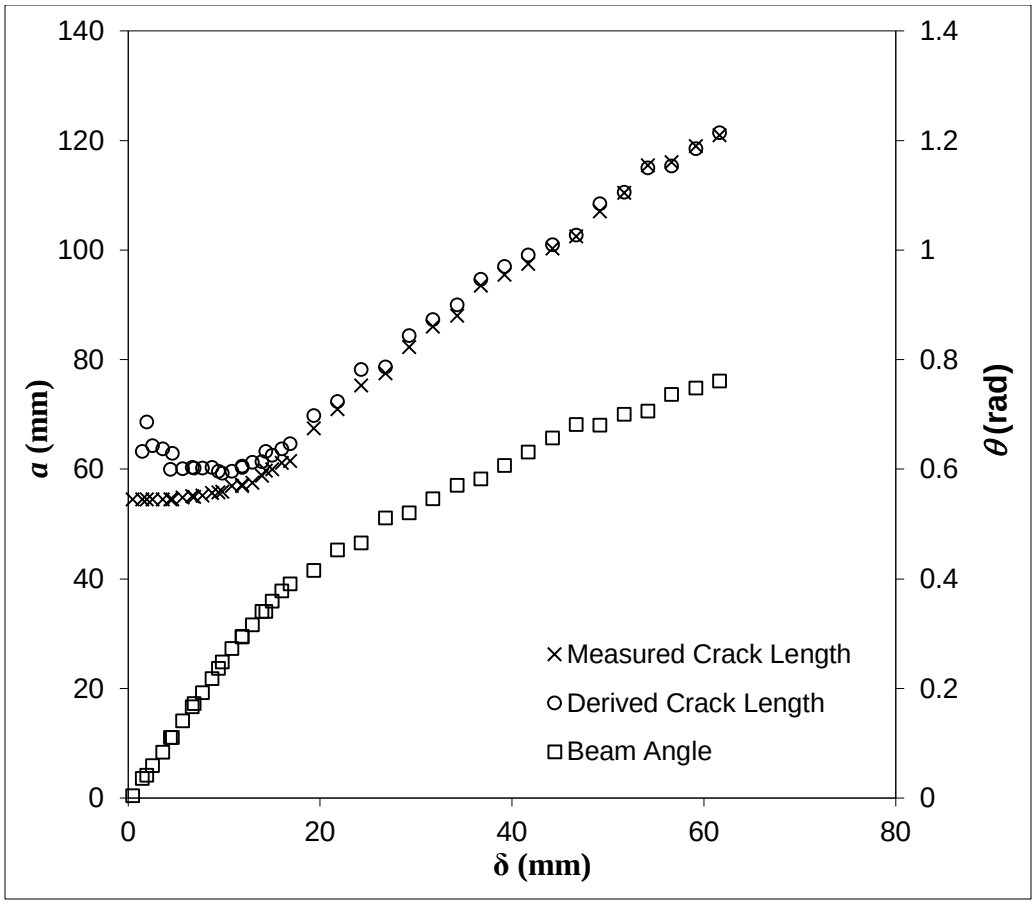

Figure 13 Measured and Derived Crack Lengths and Beam Angle vs. Load Point Displacement.

Here a is the crack length, δ is the load point displacement, and θ is the opening angle. Both critical load and ramp-up load points are shown. Equation (31) was used to calculate the derived crack length.

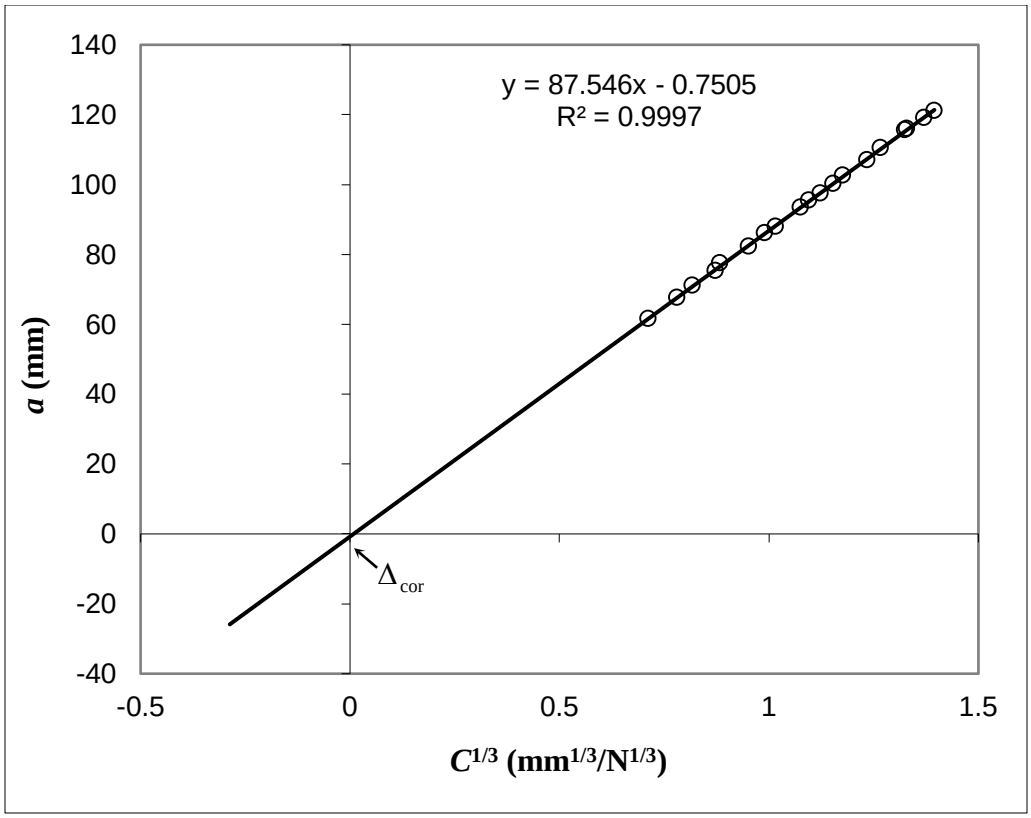

Figure 14 Determination of the Compliance Offset from the Crack Length vs. Corrected Cube Root of Compliance.

Here a is the crack length, C is the compliance, N is the correction factor from eq. 23, and Δcor is the root rotation correction introduced in eq. 21.

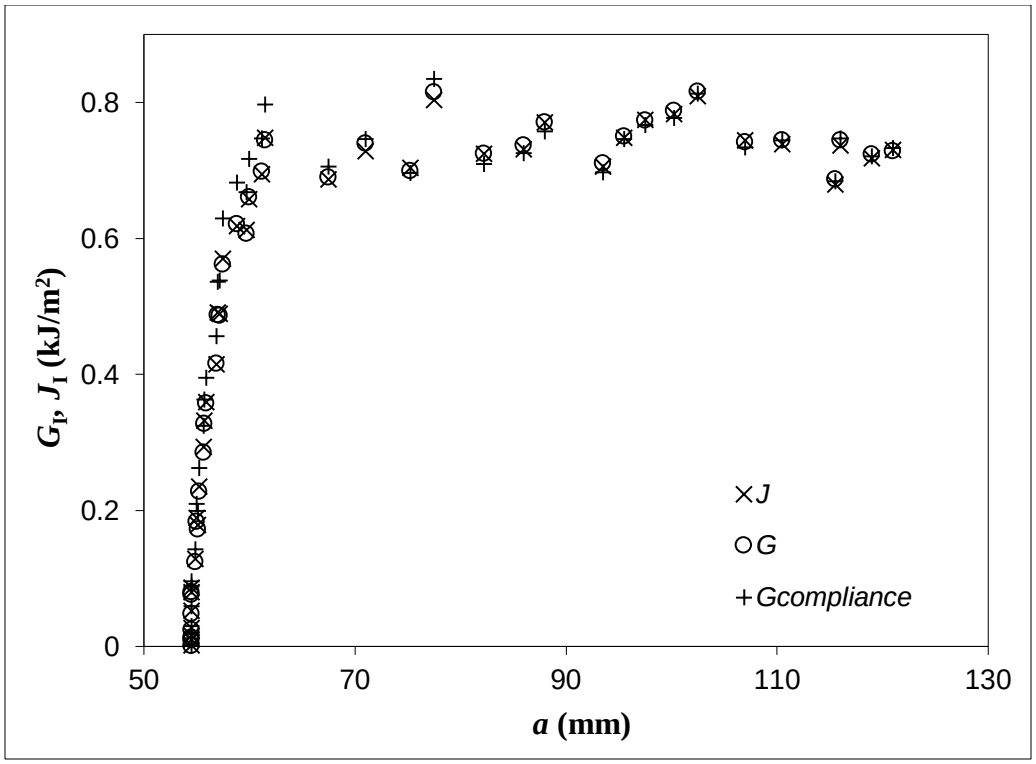

Figure 15 *G* and *J* vs. *a*.

Here a is the crack length and G_I and J_I are defined in eqs. 21 and 45 respectively.

Test 5 fracture toughness results are presented in Fig. 15 and in the Appendix, Table 1. G_I was calculated using eqs. (21-23) and measured values of P, δ, b, and a found in Figs. 1 and 2. J_I was calculated using eq. (45) and measured values of P and θ (Figs. 1 and 2). The corrected compliance equation was also plotted in Fig. 14 to determine the offset to correct for root rotation. It was found for the fifth specimen that the average value of G_{Ic} was $0.760 \pm 0.037\ \mathrm{kJ/m^2}$ and for J_{Ic} was $0.743 \pm 0.037\ \mathrm{kJ/m^2}$. The average difference between G_{Ic} and J_{Ic} was $0.97\% \pm 0.92\%$. In each case the average is given followed by the standard deviation. After the crack has advanced sufficiently, the R-curves are constant, showing neither a perceptible increasing nor decreasing trend for increasing crack length. The results for both G_{Ic} and J_{Ic} agree exceptionally well with the results of G_{Ic} calculated using the compliance method of eq. (3), the method independent

of the DCB specific theoretical analysis above, giving confidence in each method of determining the Mode I interlaminar fracture toughness.

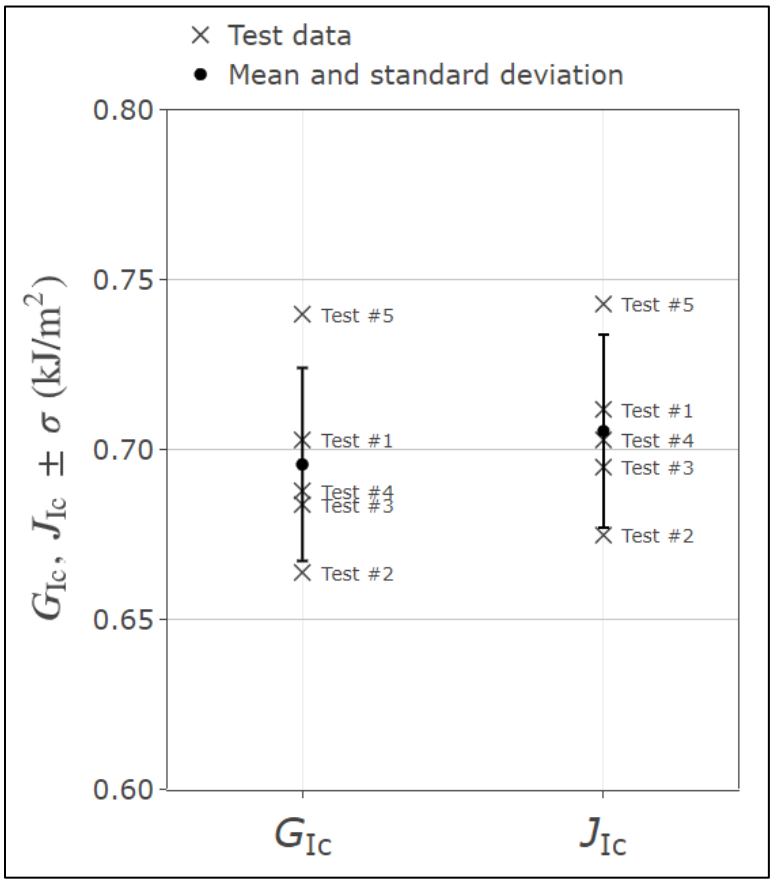

Figure 16 G_{Ic} and J_{Ic} Summary with Mean and Standard Deviation. Results of five tests are shown, with whiskers indicating standard deviation.

The results of all five tests are summarized in the Appendix, Table 2. The average difference between G_{Ic} and J_{Ic} for the series of tests was 0.97% and the standard deviation from the mean for G_{Ic} and J_{Ic} over the five tests was $0.030\ \ \mathrm{kJ/m^2}$ and $0.026\ \ \mathrm{kJ/m^2}$ respectively. These standard deviations compare favorably with those given in the ASTM standard as being typical based on round-robin testing. Furthermore, these values indicate that the variance between specimens, while relatively small, is still greater than the

variance between G_{Ic} and J_{Ic}. The ANOVA P-values for the five tests had a mean of 0.564 and a standard deviation of 0.277.

CHAPTER 5: CONCLUSIONS

Williams (1987) formulated the correction factor *F*, allowing eq. (18) to be corrected for large displacements since in standard tests neither $\overline{X}_1$ nor $\theta/2$ is measured. He states that if $\overline{X}_1$ is known and used rather than the crack length then no correction factor is needed. A root rotation correction is unnecessary since eq. (14) does not require that the beam be perfectly built in. The relationship between $\overline{X}_1$ and $\theta/2$ is tolerant of large displacements so long as the geometry and loads do not become so extreme as to violate the assumption of pure bending. Thus if $\theta/2$ is measured, it becomes possible to evaluate the large displacement fracture toughness using eq. (14) without further correction. It is precisely this formula for G_I that Williams (1987, 1989) considers the true value of G_I when developing correction factors for large displacements. Notice that eq. (14) for G_I and eq. (45) for J_I are identical. While it has long been known that G_I and J_I are identical for a small displacement analysis of linear-elastic DCB specimens, we are aware of no previous analysis showing their equivalence when the assumption of linear beam theory with small displacements is avoided.

A DCB interlaminar fracture toughness test using the *J*-integral as suggested herein removes the need to acquire visual measurements of the delamination length and avoids problems associated with locating the crack tip and crack tunneling. Also avoided are the correction factors which account for deviation from linear beam theory including geometric nonlinearity associated with large deformation and root rotation. As a

corollary, costly equipment such as a traveling microscope and the software required to automate it are replaced with inexpensive transducers. The *J*-integral DCB method allows for an instantaneous calculation of *J* applicable to a variety of material systems and is able to accommodate significant nonlinearity and/or plasticity at the crack tip. Perhaps most importantly, the method reduces the time and cost of interlaminar fracture toughness testing of composite materials while the five tests carried out in the present work show no significant difference between the results for interlaminar fracture toughness obtained by three different methods.

REFERENCES

Anderson T.L. (1991). Fracture Mechanics: Fundamentals and Applications. CRC Press

D5528-13 (2013). Standard test method for Mode I interlaminar fracture toughness of unidirectional fiber-reinforced polymer matrix composites. Annual Book of ASTM Standards 15.03

Begley J.A., Landes J.D. (1972). The *J* integral as a fracture criterion. In: Fracture Toughness Proceedings of the 1971 National Symposium on Fracture Mechanics, Part II, ASTM STP 514. American Society of Testing and Materials, 1972:1-20

Griffith A.A. (1920). The phenomena of rupture and flow in solids. Philosophical Transactions of the Royal Society of London 221(21):163-198

Gunderson J.D., Brueck, J.F., Paris A.J. (2007). Alternative test method for interlaminar fracture toughness of composites. International Journal of Fracture, 143(3):273-276

Gunderson, J.D., Paris, A.J. (2017). Suggested revisions to ASTM D5528. Presented at ASTM D30 Composite Materials Committee Meeting October 12, 2017, ASTM October 2017 Committee Week, October 8-13, 2017, Sheraton New Orleans, New Orleans, LA.

Hashemi S., Kinloch A.J., Williams J.G. (1989). Corrections needed in double cantilever beam tests for assessing the interlaminar failure of fiber composites. Journal of Materials Science Letters 8:125-129

Hertzberg R.A., Vinci R.P., Hertzberg J.L. (2013). Deformation and Fracture Mechanics of Engineering Materials. Wiley & Sons

Irwin G.R. (1948). Fracture dynamics. In: Fracturing of Metals seminar, Chicago, October 1947. American Society for Metals, Cleveland, pp 147-166

Irwin G.R., Kies J.A. (1952). Fracturing and fracture dynamics. Welding Research Supplement 31(2):95-100

Irwin G.R., Kies J.A. (1954). Critical energy rate analysis of fracture strength. The Welding Journal 33(4):193-198

Nilsson F. (2006). Large displacement aspects on fracture testing with double cantilever beam specimens. International Journal of Fracture, 139:305-311

Orowan E. (1950). Fundamentals of brittle behavior in metals. In: Murray W M (ed) Fatigue and fracture of metals: Symposium held at the Massachusetts Institute of Technology, June 1950. The Technology Press of The Massachusetts Institute of Technology and John Wiley & Sons Inc., New York, pp 139-167

Paris A.J., Paris P.C. (1988). Instantaneous evaluation of J and C*. International Journal of Fracture 38(1):19-21

Rice J.R. (1968). A path independent integral and the approximate analysis of strain concentration by notches and cracks. Journal of Applied Mechanics 35:379-386

Williams J.G. (1989). The fracture mechanics of delamination tests. Journal of Strain Analysis 24(4):207-214

Williams J.G. (1987). Large displacements and end block effects in the DCB interlaminar test in Modes I and II, Journal of Composite Materials 21:330-347

APPENDIX

Table 1 Test 5 Data

Ramp-Up						Propagation					
δ	**P**	**a**	**θ**	**J_{IC}**	**G_{IC}**	**δ**	**P**	**a**	**θ**	**J_{Ic}**	**G_{Ic}**
mm	N	mm	rad	kJ/m²	kJ/m²	mm	N	mm	rad	kJ/m²	kJ/m²
0.4	2.49	54.5	0.004	0.000	0.001	11.88	41.79	57.00	0.295	0.488	0.491
1.5	6.33	54.5	0.036	0.009	0.010	14.38	45.08	59.75	0.341	0.607	0.613
2.5	10.24	54.5	0.059	0.024	0.027	16.87	48.20	61.50	0.391	0.744	0.748
3.5	14.26	54.5	0.084	0.048	0.053	19.36	42.12	67.50	0.416	0.690	0.687
4.6	18.18	54.5	0.110	0.079	0.087	21.85	41.53	71.00	0.453	0.740	0.728
5.6	22.17	54.9	0.141	0.124	0.128	24.31	38.15	75.25	0.466	0.699	0.704
6.6	26.08	55.1	0.166	0.172	0.178	26.79	40.67	77.50	0.511	0.815	0.804
7.7	29.90	55.3	0.192	0.228	0.235	29.28	35.52	82.25	0.520	0.725	0.725
8.7	33.06	55.7	0.218	0.285	0.293	31.77	34.46	86.00	0.546	0.737	0.731
9.8	36.37	55.9	0.248	0.357	0.359	34.26	34.46	88.00	0.571	0.771	0.771
10.8	38.62	56.9	0.272	0.416	0.415	36.75	31.18	93.50	0.582	0.710	0.705
11.8	41.76	57.2	0.294	0.486	0.489	39.24	31.61	95.50	0.607	0.750	0.748
						41.72	31.40	97.50	0.632	0.774	0.774
						44.21	30.76	100.25	0.657	0.788	0.783
						46.70	30.76	102.50	0.681	0.816	0.809
						49.19	28.01	107.00	0.680	0.742	0.744
						51.67	27.30	110.50	0.701	0.744	0.739
						54.16	25.02	115.50	0.706	0.687	0.680
						56.65	26.04	116.00	0.737	0.744	0.737
						59.15	24.92	119.00	0.749	0.723	0.718
						61.63	24.71	121.00	0.761	0.728	0.730

Table 2 Combined Data for 5 Tests

	1	2	3	4	5	Mean	Std. Dev.
G_{Ic} (kJ/m^2)	0.719	0.682	0.695	0.699	0.760	0.711	0.0304
J_{Ic} (kJ/m^2)	0.712	0.673	0.690	0.701	0.743	0.704	0.0262
Difference (%)	0.970	1.275	0.709	-0.311	2.213	0.971	0.915
ANOVA P	0.704	0.388	0.690	0.865	0.176	0.564	0.277